Fabrication of Pd-Nb bimetallic doped organosilica membranes by different metal doping routes for H2/CO2 separation

Hengfei Zhang, Yibin Wei, Shufeng Niu, Hong Qi

PII: S1004-9541(20)30477-8

DOI: https://doi.org/10.1016/j.cjche.2020.09.003

Reference: CJCHE 1907

To appear in: *Chinese Journal of Chemical Engineering*

Received date: 8 June 2020

Revised date: 16 August 2020

Accepted date: 6 September 2020

Please cite this article as: H. Zhang, Y. Wei, S. Niu, et al., Fabrication of Pd-Nb bimetallic doped organosilica membranes by different metal doping routes for H2/CO2 separation, *Chinese Journal of Chemical Engineering* (2020), https://doi.org/10.1016/j.cjche.2020.09.003

Fabrication of Pd-Nb bimetallic doped organosilica membranes by different metal doping routes for H_2/CO_2 separation

Hengfei Zhang [a], Yibin Wei [a], Shufeng Niu [b], Hong Qi [a, *]

[a] *State Key Laboratory of Material-Oriented Chemical Engineering, Membrane Science and Technology Research Center, Nanjing Tech University, Nanjing 210009, China*

[b] *Hongyi Ceramic Membranes Research Institute, Nanjing Hongyi Ceramic Nanofiltration Membranes Co., Ltd. Nanjing 210009, Jiangsu, China*

** Tel. +86-25-83172279; Email: hqi@njtech.edu.cn*

Abstract

Monometallic doping has proved its superiority in improving either permselectivity or H_2 permeability of organosilica membranes for H_2/CO_2 separation, but it is still challenging to break the trade-off effect. Herein, we report a series of Pd-Nb bimetallic doped 1,2-bis(triethoxysilyl)ethane (Pd-Nb-BTESE, PNB) membranes with different metal doping routes for simultaneously improving H_2 permeance and H_2/CO_2 permselectivity by the synergetic effects of Pd and Nb. The doped Pd can exist in the BTESE network as nanoparticles while the doped Nb is incorporated into BTESE network forming Nb-O-Si covalent bonds. The metal doping routes significantly influence the microstructure of PNB networks and gas separation performance of the PNB membranes. We found that the PNB membrane with Pd doping priority (PNB-Pd) exhibited the highest surface area and pore volume, comparing with Nb doping priority (PNB-Nb) or Pd-Nb simultaneous doping (PNB-PdNb). The PNB-Pd membrane could not only exhibit an excellent H_2 permeance of ~10^{-6} mol·m^{-2}·s^{-1}·Pa^{-1} but also a high H_2/CO_2 permselectivity of 17.2. Our findings may provide novel insights into preparation of bimetallic doped organosilica membranes with excellent H_2/CO_2 separation performance.

Keywords: Hydrogen; Separation; Membranes; Bimetallic doping; Organosilica.

1. Introduction

As the new generation of silica-based membranes, organosilica membranes containing both organic and inorganic compositions have been considered promising for H_2/CO_2 separation [1]. The rigid inorganic linkages of Si-O-Si bonds provide high mechanical strength and thermal stability, meanwhile the organic linkages of Si-R-Si (R represents organic groups) enhance the flexibility and hydrophobicity of organosilica membranes [2]. Multifarious organic bridging groups, including the alkylene (e.g. CH_2, C_2H_2 and C_8H_{16}) and the aromatic (e.g. benzene and biphenyl), confer organosilica membranes family with versatility and tailoring pore structures properties [3-5].

In recent years, 1,2-bis(triethoxysilyl)ethane (BTESE)-derived organosilica membranes with flexible Si-C-C-Si linkages have been widely investigated for small molecule gases separation due to its good molecular sieving performance and hydrothermal stability [6]. Kanezashi et al. [7] first reported that BTESE-derived membranes could be used for H_2/CO_2 separation and found that the H_2 permeance of BTESE membrane could reach up to ~10^{-5} mol·m^{-2}·s^{-1}·Pa^{-1}. However, their H_2/CO_2 permselectivity was very low, which was close to Knudsen factor (4.7). The poor H_2/CO_2 permselectivity is ascribed to the larger pore size caused by the longer Si-C-C-Si bonds in the BTESE-derived network [8]. Therefore, improving H_2/CO_2 permselectivity yet remaining high H_2 permeance of BTESE-derived membranes have attracted much interest for researchers.

Metal doping that could not only tailor pore structure but also trigger interactions with H_2 or CO_2 molecules has been considered as a promising strategy to improve H_2/CO_2 separation performance for silica-based membranes. Metals such as Co, Mg, Al, Zr, Nb, Pd

and etc., have been successfully introduced in silica-based networks (e.g. pure silica and organosilica) [9-17]. Generally, the doped metals could exist in silica-based networks as two forms: (1) covalent bonds connected with silica-based network (M-O-Si, M represents metal), (2) metal or metal oxides nanoparticles embedded into silica-based network. Song et al. [13] prepared Zr doped BTESE (Zr-BTESE) membranes by using zirconium alkoxides as the metal source, and found that the Zr-BTESE membrane could exhibit a lower H_2 permeance of 1.15×10^{-8} mol·m^{-2}·s^{-1}·Pa^{-1} but a higher H_2/CO_2 permselectivity of 23 than the performance of pure BTESE membrane (H_2 permeance of 5×10^{-7} mol·m^{-2}·s^{-1}·Pa^{-1}, H_2/CO_2 permselectivity of 4). They confirmed that the result could be attributed to the formation of Zr-O-Si bonds in the Zr-BTESE network. A similar result was also found by Qi et al. [15] that doping Nb into BTESE-derived network could lead to the formation of Nb-O-Si covalent bonds, making the network become relatively dense. The optimal Nb-BTESE membrane also showed a high H_2/CO_2 permselectivity of 121, but a low H_2 permeance of 5.1×10^{-8} mol·m^{-2}·s^{-1}·Pa^{-1}. Thus, when a specific metal is doped into a silica-based network forming covalent bonds, the obtained network usually becomes dense and the corresponding membrane generally shows a high H_2/CO_2 permselectivity but a low H_2 permeance.

On the other hand, Kanezashi et al. [18] attempted to dope Pd into tetraethoxysilane (TEOS)-derived silica (Pd-TEOS) membranes for improving H_2/CO_2 separation performance. They found that the doped Pd existed in the silica networks as nanoparticles, which significantly improve the H_2 permeance of the membrane. Although Pd-TEOS membranes could exhibit the enhanced H_2 permeance, the H_2/CO_2 permselectivities were still very low. Because some large pores were formed at the interface between the formed Pd nanoparticles

and the silica network due to the poor compatibility. Our group [17] also confirmed that Pd could be doped into BTESE-derived organosilica (Pd-BTESE) membranes as nanoparticles. The membrane showed a high H_2 permeance of 7.26×10^{-7} mol·m^{-2}·s^{-1}·Pa^{-1} and a low H_2/CO_2 permselectivity of 4.3, and the results could be attributed to the enlarged pore size of Pd-BTESE membrane and increased H_2 adsorption by the Pd nanoparticles. Therefore, the randomly distributed Pd nanoparticles are beneficial to improve the H_2 permeance due to the strong adsorbability and solvability of Pd towards H_2 [19].

As introduced above, doping different metals into silica-based membranes with different mechanisms can significantly change the ultimate H_2/CO_2 separation performance of the membranes. Unfortunately, most metal-doped silica membranes were based on monometallic doping [20] and the monometallic doping strategy was proved difficult to break through the trade-off limitation between H_2 permeance and H_2/CO_2 permselectivity. Despite the bimetallic doping strategy has been proposed for improving the gas separation performance of silica-based membranes [21-25], these works focused on improving the poor hydrothermal stability of TEOS-derived silica membranes using Co as the main metal. Very recently, Zhang et al. [26] reported the first bimetallic doped organosilica membranes by doping La-Y into BTESE-derived networks for the application of desalination, they found that La and Y could both form Si-O-M (M represents La and Y) bonds in the organosilica networks.

Inspired by the two metal doping mechanisms, recently, we successfully prepared bimetallic Pd-Nb doped BTESE (Pd-Nb-BTESE) membranes with excellent H_2/CO_2 separation performance by taking advantages of the synergetic effects of the two metals [27]. We found that when incorporated Pd into Nb-induced organosilica networks, the formed Pd

nanoparticles can not only inhibit excessive densification of Nb-doped networks, but also confer the networks with strong H_2 adsorbability. Therefore, in this study, three metal doping routes (i.e. Pd doping priority, Nb doping priority and Pd-Nb simultaneous doping) were chosen to optimize the performances of this novel Pd-Nb-BTESE membrane. The properties of these membranes, such as the chemical states of Nb and Pd in the membrane, microstructures and H_2/CO_2 separation performance were investigated in detail. Bimetallic doping mechanisms with respect to this Pd-Nb-BTESE membrane were preliminarily revealed.

2. Experimental

2.1. Materials

1,2-bis (triethoxysilyl) ethane (BTESE, purity 97%) was purchased from ABCR GmbH. Palladium chloride ($PdCl_2$, purity 98%) and Niobium penta (n) butoxide (NPB, purity 99%) were purchased from Meryer (Shanghai) Chemical Technology Co., Ltd.. Ethanol anhydrous (EtOH, purity 99.9 %) and hydrochloric acid (HCl, 36.5 wt%) were purchased from Merck Corporation and Liyang Oriental Chemical Reagent Co., Ltd., respectively. Prior to further use, the concentrated HCl was diluted to 1 M with deionized (DI) water (5 $\mu S \cdot cm^{-1}$ at 25 ºC). Home-made disc-type γ-Al_2O_3 mesoporous membranes (thickness: 2.5 mm, diameter: 42 mm, pore size: 3-5 nm) were used as the supports.

2.2. Synthesis of Pd-Nb-BTESE sols

The synthetic processes of Pd-Nb doped BTESE (PNB) sols with different metal doping routes are shown in Fig. 1. BTESE sol, $PdCl_2$ solution and NPB solution were first synthesized, respectively. Typically, 5 mL BTESE and 5 mL EtOH were first mixed in a

nitrogen glove-box. 0.5 mL HCl solution (1 M) was then drop-wise added into the BTESE-EtOH mixture under vigorous stirring in an ice bath. Finally, the mixture was refluxed in a water bath at 60 ºC for 90 min to obtain pure BTESE sol. 0.383 g $PdCl_2$ powders were dissolved with 0.72 mL HCl (36.5 wt%) in a water bath at 60 ºC for 40 min, then the mixture was diluted with 30 mL EtOH to obtain $PdCl_2$ solution. The NPB solution was prepared by diluting 0.226 mL NPB with 20 mL EtOH in a nitrogen glove-box.

30.72 mL $PdCl_2$ solution and 5 mL EtOH mixture were added into the 3.1 mL BTESE sol to form the Pd-BTESE mixture, then the Pd-BTESE mixture was refluxed in a water bath at 60 ºC for 90 min to obtain the Pd-BTESE sol. The full NPB solution, 0.3 mL HCl (1 M) and 5 mL EtOH were added into the resulting Pd-BTESE sol for refluxing at 60 ºC for 90 min to obtain a PNB sol. As Pd metal was first introduced into BTESE sol and Nb metal was sequentially doped into the Pd-BTESE sol, the synthesized sol was denoted as PNB-Pd. Similarly, the PNB sol with Nb doping priority was denoted as PNB-Nb. When $PdCl_2$ and NPB solutions were simultaneously added into the pure BTESE sol, the mixture sol was denoted as PNB-PdNb. The molar ratio of the three PNB sols was controlled as the same (Si: Pd: Nb: H_2O: HCl: EtOH = 1: 0.4: 0.1: 9.65: 1.65: 197).

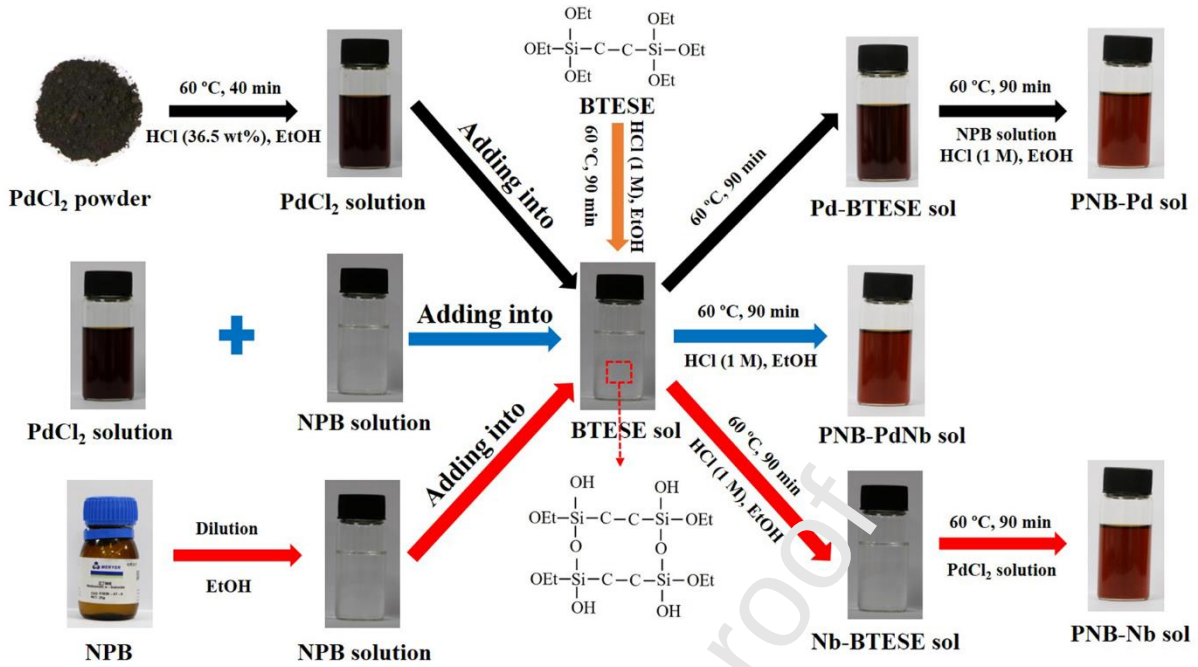

Fig. 1. Schematic illustration of the synthesis process of sols with different metal doping routes. The orange, black, red and blue arrows link to the synthetic routes of BTESE, PNB-Pd, PNB-Nb and PNB-PdNb sols, respectively.

2.3. Preparation of PNB membranes

The PNB-Pd, PNB-Nb and PNB-PdNb membranes were prepared by single dip-coating the corresponding PNB sols onto γ-Al_2O_3 supports, respectively. Then the freshly coated membranes were dried in a humidity chamber (40 ºC, 25% relative humidity) for 3 h. Finally, the membranes were calcined at 400 ºC for 3 h with the same heating and cooling rate of 0.5 ºC·min^{-1} in a tube furnace (GHA 12/1050, Carbolite). A reductive calcination atmosphere of H_2/N_2 (2:3 in molar ratio) was used.

The as-prepared three PNB sols were dried in petri dishes at room temperature for 24 h. Next, the obtained xerogels were ground into fine powders and then calcined in the same conditions as for the preparation of PNB membranes. The obtained PNB powder samples were used for characterization to indicate the properties of the corresponding membranes.

2.4. Characterization

Crystalline structures of the PNB powder samples were analyzed by an X-ray diffractometer (XRD, MiniFlex 600, Rigaku) using Cu Kα radiation at 40 kV and 15 mA. Fourier transform infrared (FTIR) spectroscopy (NICOLET 8700, Thermo Nicolet Corporation) with KBr tablet method and X-ray photoelectron spectroscopy (XPS, ESCALAB250xi, Thermo Scientific) equipped with a monochromatic Al Kα X-ray source (1486.6 eV) were used to analyze the chemical states of the PNB powders. The surface and cross-sectional morphologies of membranes were observed by a scanning electron microscopy (SEM, S-4800, Hitachi) with the accelerating voltage of 7 kV. The morphologies of the as-prepared PNB networks were observed by a high-resolution transmission electron microscope (HRTEM, JEM-200CX, JEOL). The particle size distribution in the TEM images was measured by a Nano Measurer 1.2 software. Microstructural properties of the as-prepared membranes were characterized by analyzing the N_2 adsorption-desorption isotherms (ASAP 2020, Micromeritics) of the corresponding powder samples at -196 ºC. Before gas adsorption measurement, samples were degassed under vacuum at 200 ºC for 12 h. The pore size distributions of PNB membranes were calculated by the non-local density functional theory (NLDFT) method. H_2 and CO_2 gas adsorption isotherms at 25 ºC for the as-prepared powder samples were also studied.

2.5. Evaluation of gas separation performance

The single gas permeances of He, H_2, CO_2, CH_4, N_2 and SF_6 were measured from 50 to 200 ºC on a home-made apparatus. The detailed information of the apparatus can be found elsewhere [17]. The gas permeance was calculated according to the Eq. (1):

$$P_i = \frac{F_i}{A\,\Delta P} \quad (1)$$

where P_i is the permeance of gas i (mol·m^{-2}·s^{-1}·Pa^{-1}), F_i is the flow rate (mol·s^{-1}), A is the effective membranes area (m^2), ΔP is the transmembrane pressure (Pa).

The ideal separation factor (α) was calculated by the Eq. (2):

$$\alpha = \frac{P_i}{P_j} \quad (2)$$

where P_i and P_j are the permeance of gas i and j, respectively.

3. Results and discussion

3.1. Chemical composition analysis of PNB membranes

Fig. 2 (a) shows the XRD patterns of the three PNB networks obtained by different synthetic routes. We found that the XRD patterns of the three PNB networks were identical. No Nb-related diffraction peaks were detected in the three XRD patterns, indicating that niobium compounds are amorphous in the organosilica network. This result is consistent with our previous study on Nb monometallic doped BTESE membranes that Nb was well dispersed into organosilica network [28]. The peaks at 40.14 º, 46.7 º and 68.18 º are ascribed to (111), (200) and (220) planes of Pd (0) [29]. The detected Pd (0) diffraction peaks suggested that Pd (2+) were reduced in the presence of H_2/N_2 atmosphere at 400 ºC, which are consistent with our previous work [30]. Fig. 2 (b) shows the FTIR spectra of PNB networks obtained by different synthetic routes. The three samples exhibited similar FTIR spectra confirming that chemical composition of the three PNB membranes are similar. The peaks at 3450, 2905, 1628, 775 and 680 cm^{-1} correspond to Si-OH stretching vibrations, -CH_2 stretching vibrations, H-O-H deformation vibrations, -CH_2 rocking vibrations and Si-C stretching vibrations, respectively [31, 32]. The two peaks at 1410 and 1426 cm^{-1} are assigned

to bending asymmetric vibrations of $-CH_2$ for $-CH_2-CH_2-$, confirming the existence of ethane-bridged $Si-CH_2-CH_2-Si$ groups [32]. The broad band at 1040 cm^{-1} is ascribed to asymmetric stretching vibration of Si-O-Si which were formed by the polymerization reaction of Si-OH groups [31].

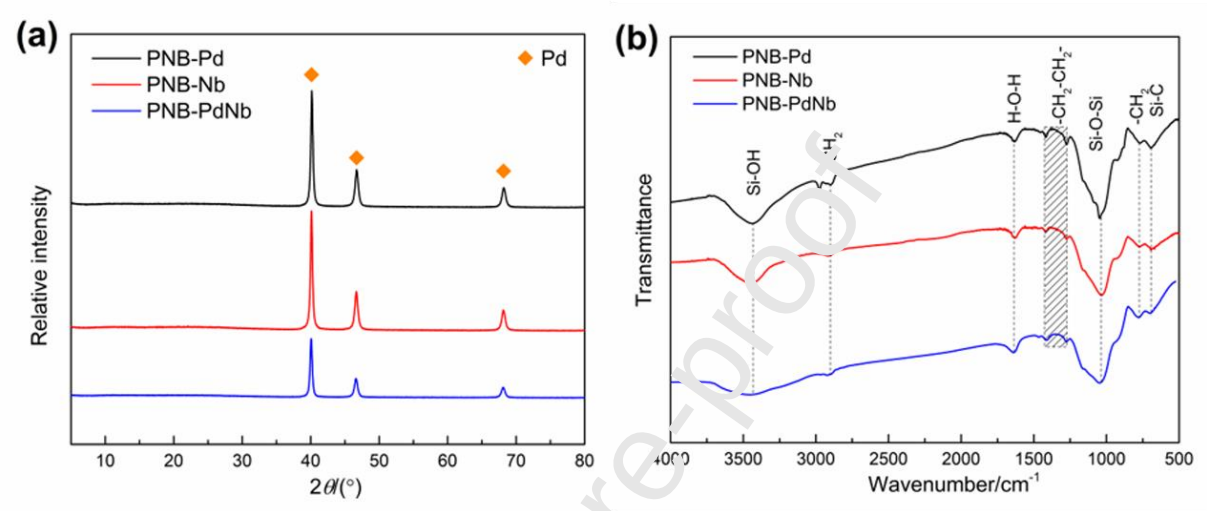

Fig. 2. (a) XRD patterns and (b) FTIR spectra of PNB powders.

For further investigating the condensation degree of silanol groups, the FTIR absorption peaks of PNB samples at the range of 850-1200 cm^{-1} were deconvoluted into six peaks by Gaussian function to identify the overlapping bands of Si-O-Si and Si-OH bands (Fig. 3) [26]. The peaks center at around 1160, 1115, 1055 and 1005 cm^{-1} (i.e. peak 1-4) were ascribed to Si-O-Si stretching vibration, while the peaks at 917 and 880 cm^{-1} (i.e. peak 5 and 6) correspond to Si-OH bending vibration [33]. The FTIR peak area ratio of Si-O-Si to Si-OH groups is considered as the indicator of the condensation degree for PNB networks [26], and the condensation (also known as cross-linking) degree of silica networks is closely related to the pore structure of silica-based membranes [34]. The PNB-Pd and PNB-Nb networks displayed much higher Si-O-Si/Si-OH peak area ratios than that of PNB-PdNb. This result

may indicate that one-by-one bimetallic doping (i.e. PNB-Pd or PNB-Nb) is more favorable to increase the cross-linking degree of PNB networks than the route of simultaneous doping with two metals (i.e. PNB-PdNb).

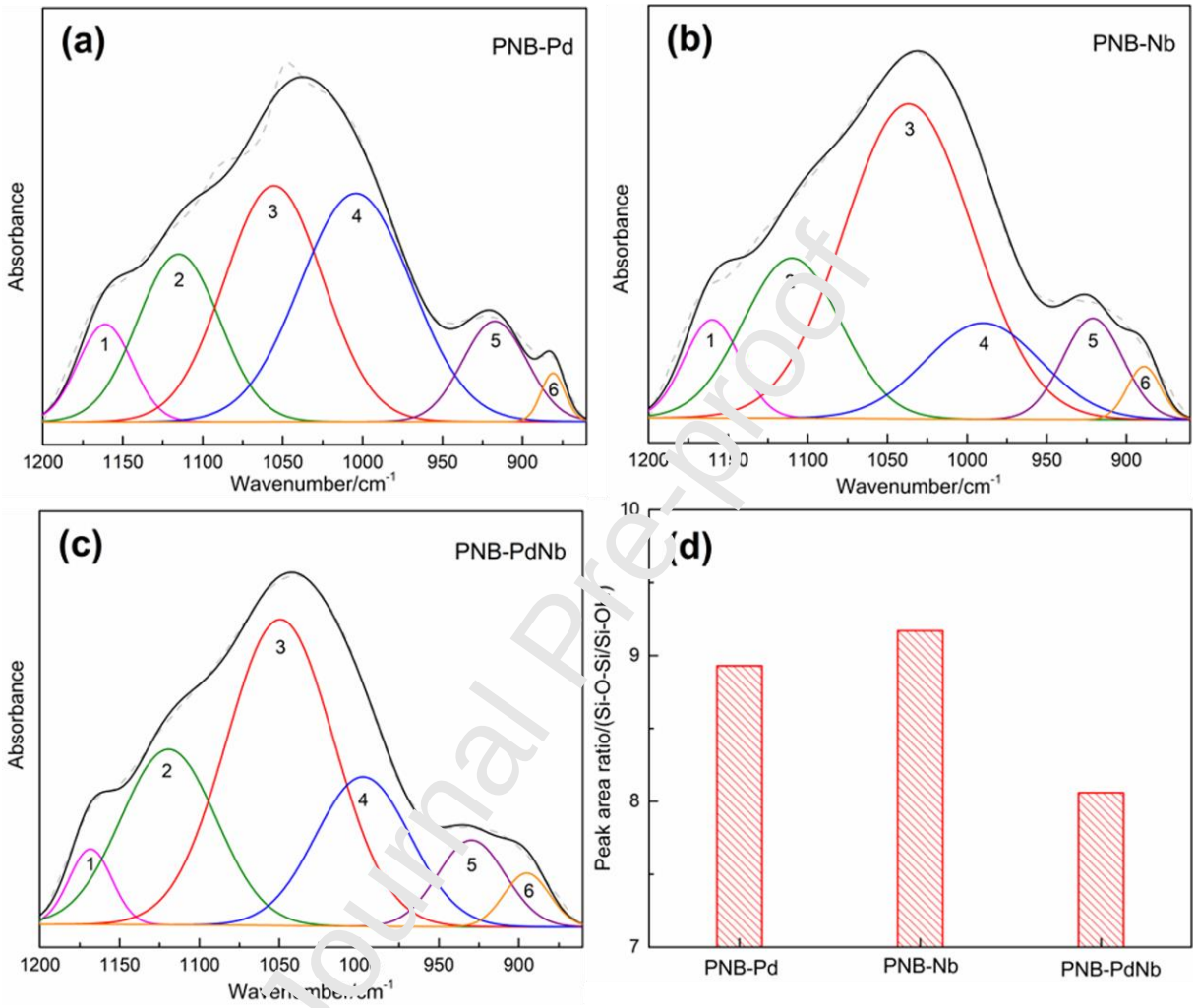

Fig. 3. The deconvolution of FTIR spectra of (a) PNB-Pd, (b) PNB-Nb, (c) PNB-PdNb powders, and (d) Si-O-Si/Si-OH peak area ratios for the three networks.

To confirm the chemical states of Nb in the three organosilica networks, the Nb 3d core-level XPS spectra of PNB-Pb, PNB-Nb, PNB-PdNb networks and pure Nb_2O_5 powder were analyzed (Fig. 4). The XPS spectra of Nb 3d were deconvoluted into two peaks at binding energies of 208.2 eV and 210.9 eV, which correspond to Nb $3d_{5/2}$ and Nb $3d_{3/2}$,

respectively. The binding energies of Nb $3d_{5/2}$ and Nb $3d_{3/2}$ for PNB powders are higher than those of pure Nb_2O_5 (Nb $3d_{5/2}$ of 207.2 eV and Nb $3d_{3/2}$ of 209.9 eV). This chemical shift indicated that niobium atoms were incorporated into BTESE networks forming Nb-O-Si covalent bonds, corroborating with previous reports [35-37].

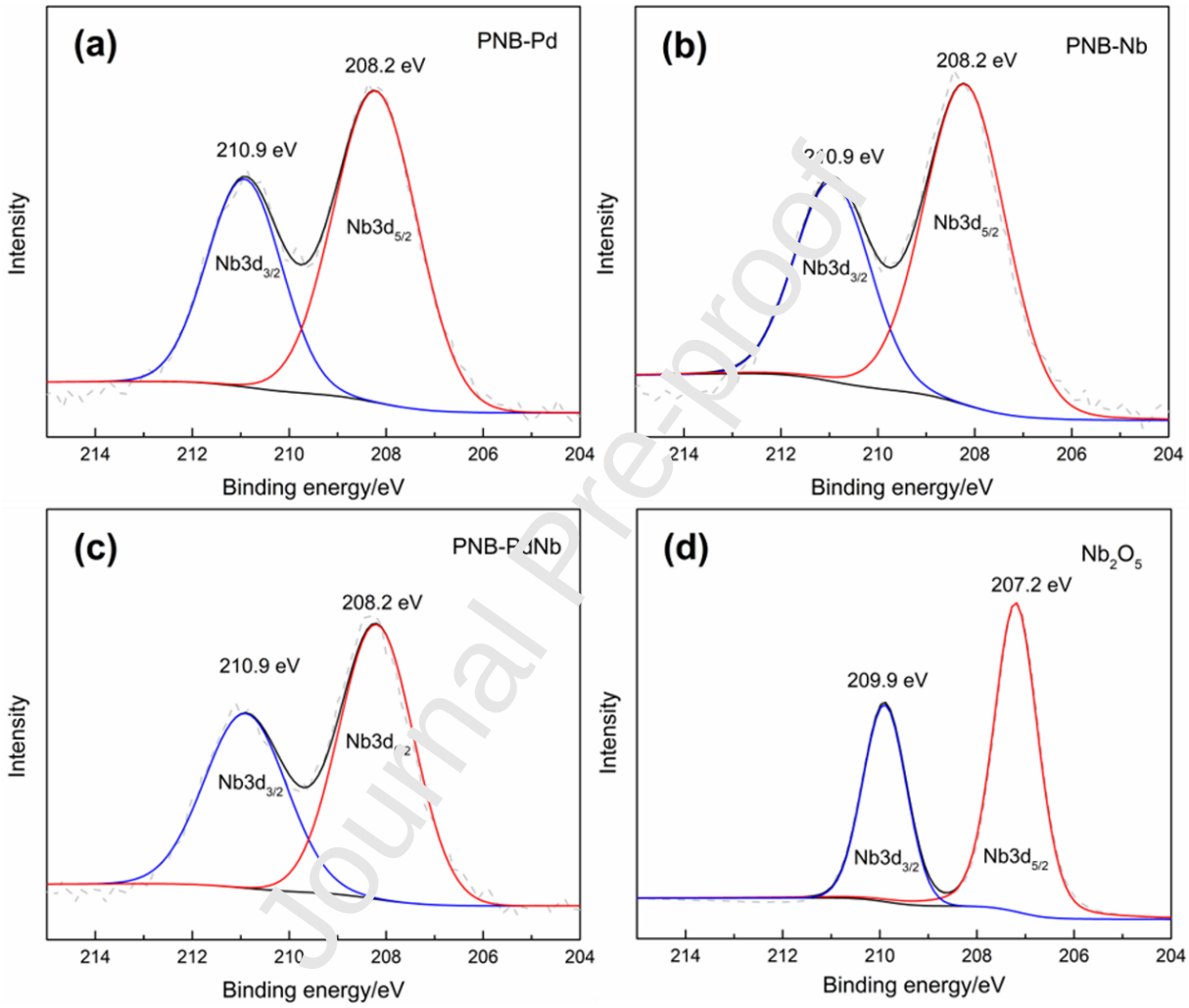

Fig. 4. XPS spectra for Nb 3d of (a) PNB-Pd, (b) PNB-Nb, (c) PNB-PdNb and (d) Nb_2O_5 powders.

3.2. Morphological and microstructural analysis of PNB membranes

Fig. 5 shows the morphologies and the size distributions of Pd nanoparticles for the three PNB membranes. We observed that Pd nanoparticles were randomly embedded into the three

organosilica networks, however, the size distributions of Pd nanoparticles for the three networks were different. The Pd nanoparticle size distribution for the PNB-Pd network was mainly concentrated on 10-20 nm. Interestingly, the size of Pd nanoparticles in PNB-Nb network were smaller within the range of 2-6 nm. In addition, the PNB-PdNb network displayed an irregular size distribution for Pd nanoparticles with both small particles and large particles in the ranges of 5-10 nm and 15-25 nm, respectively.

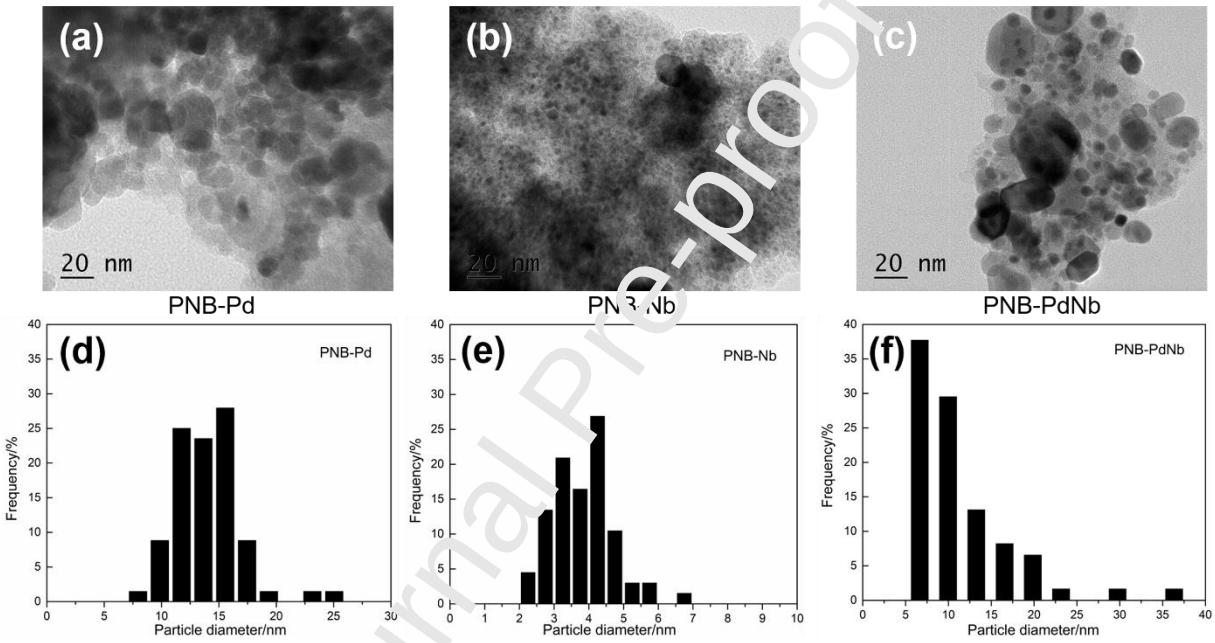

Fig. 5. HRTEM images and particle size distribution of PNB powders.

Fig. 6 shows the hypothetical structures of the PNB membranes prepared by the three synthetic routes. Based on the findings of Pd or Nb monometallic doped BTESE networks in our previous studies [15, 17], Nb-doped BTESE networks are generally denser than that of the pure BTESE network and exhibit relatively smaller pore size, due to the formation of Nb-O-Si bonds. Pd can be doped into BTESE-derived networks in the form of nanoparticles. The relatively large pore size and low cross-linking degree of pure BTESE network is beneficial for the growth of large Pd nanoparticles due to the weak space resistance. Therefore,

the uniformly large Pd nanoparticles could be found in the PNB-Pd network. On the other hand, when Nb is first doped into the BTESE network, the dense Nb-BTESE network with small pore size may provide strong space resistance, resulting in the formation of smaller Pd nanoparticles in the PNB-Nb network after Pd doping. When Pd and Nb are simultaneously doped, we hypothesize that Pd nanoparticles may be confined within both pure BTESE network as the large particles and the Nb-BTESE network as the small particles, respectively, leading to the irregular particle size distribution of the PNB-PdNb network.

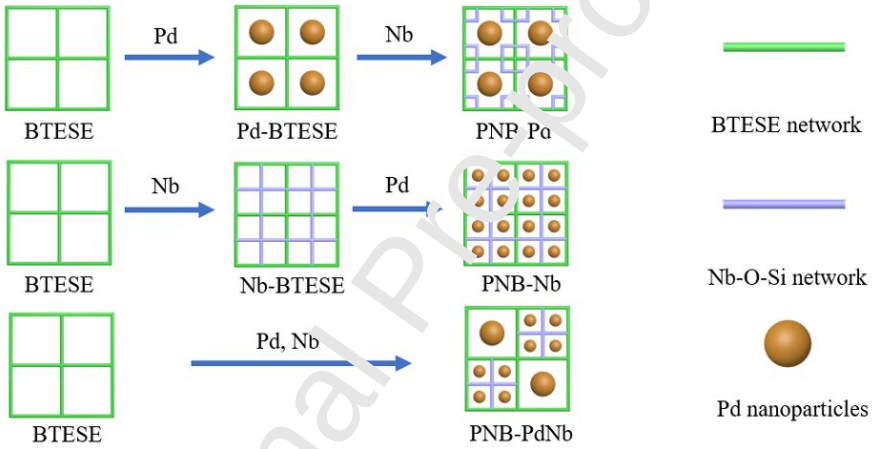

Fig. 6. Schematic illustration of the hypothetical structures of the PNB networks with different synthetic routes.

Fig. 7 shows the surface and cross-sectional morphologies of the three PNB membranes. As the typical PNB membrane, the PNB-Pd membrane has a smooth and defect-free surface, and an asymmetric structure including a α-Al_2O_3 support layer, a γ-Al_2O_3 intermediate layer and a PNB separation layer was imaged (Fig. 7 (a)-(c)). The morphologies of the three PNB membranes are similar with an ultrathin PNB separation layer with the thickness of about 100 nm.

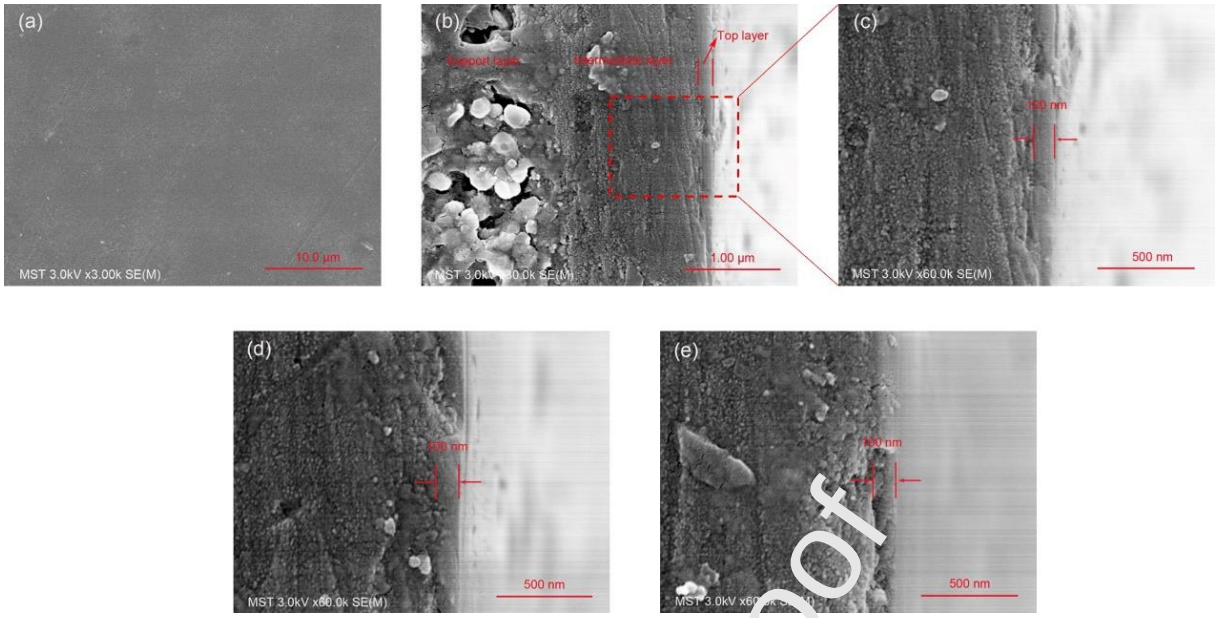

Fig. 7. SEM images of (a)-(c) PNB-Pd membrane observed from top and cross-section. (d) and (e) are cross-sectional SEM images of PNB-Nb and PNB-PdNb membranes.

N_2 adsorption-desorption experiments were conducted to determine the effects of the three metal doping routes on the microstructural properties of the corresponding PNB networks. In Fig. 8, the N_2 adsorption-desorption isotherms of all samples showed a rapid rise at very low relative pressure. This characteristic matches well with type I isotherms, confirming that the three PNB membranes have microporous structures [38]. Notably, the PNB-PdNb network exhibited an obvious hysteretic loop in the range of 0.4-1 relative pressure, suggesting the existence of relatively large volume of mesopores. Combined with the aforementioned FTIR and TEM analysis, the result may be attributed to the low condensation degree of Si-O-Si/Si-OH and the irregular size distribution of Pd nanoparticles in the PNB-PdNb network. The Brunauer-Emmett-Teller surface area (S_{BET}) and total pore volume (V_{total}) of PNB powders are provided in Table 1. PNB-Pd powders showed the highest S_{BET} (335 $m^2 \cdot g^{-1}$) and V_{total} (0.201 $cm^3 \cdot g^{-1}$) compared with the PNB-Nb and PNB-PdNb

samples. This result indicates that the Pd doping priority is favorable to enhance the porosity of the PNB-Pd membrane, because the large Pd nanoparticles confined in the BTESE network can expand the structure of its networks. On the contrary, the S_{BET} and V_{total} of PNB-Nb powders were the smallest suggesting that the Nb doping priority leads to the formation of dense structure. Because of the relatively dense network of Nb-BTESE, the formed small Pd nanoparticles are not able to expand the PNB-Nb network. Moreover, the PNB-PdNb network exhibited a compromise S_{BET} and V_{total} of 252 $m^2 \cdot g^{-1}$ and 0.176 $cm^3 \cdot g^{-1}$, respectively.

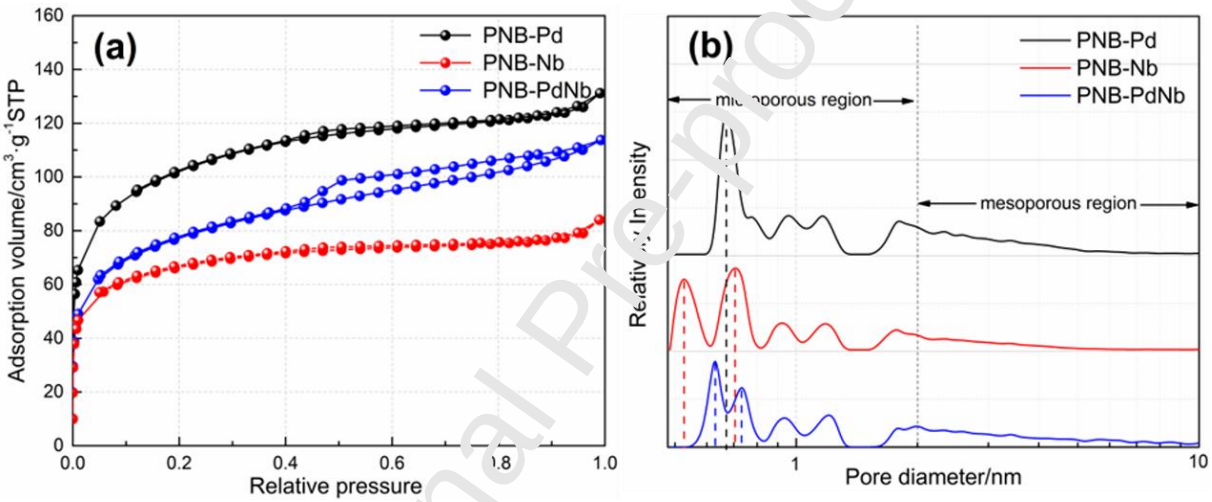

Fig. 8. (a) N_2 adsorption-desorption isotherms and (b) pore size distributions of PNB membranes.

Table 1 Pore structure data of PNB powders

Sample	S_{BET} ($m^2 \cdot g^{-1}$)	V_{total} ($cm^3 \cdot g^{-1}$)
PNB-Pd	335	0.201
PNB-Nb	213	0.132
PNB-PdNb	252	0.176

Note: S_{BET} and V_{total} represent Brunauer-Emmett-Teller (BET) surface area and total pore volume, respectively.

The pore size distributions of the PNB-Pd, PNB-Nb and PNB-PdNb networks were

further analyzed using the NLDFT model (Fig.8 (b)). All samples exhibited the multimodal pore size distributions proving the existence of the hierarchically porous structure for the PNB membranes. The pore size distribution of PNB-Pd network was mainly centered at 6.72 Å. However, both the PNB-Nb and the PNB-PdNb networks exhibited two peaks in their pore size distributions, the pore size peaks for the former were at 5.28 and 7.07 Å, the pore size peaks for the latter were a little larger (6.29 and 7.33 Å). These pore size analytical results partially match with the aforementioned FTIR and TEM analysis, providing supportive evidences for our hypothesis of the PNB networks that synthesized by different metal doping routes.

3.3. Gas separation performance of PNB membranes

Fig. 9 shows the gas permeance of PNB membranes prepared by different metal doping routes. Obviously, the permeances of the three PNB membranes exhibited a decreasing tendency as the kinetic diameter of gases increases, proving their molecular sieving properties. We note that the high H_2 permeances for the three membranes were attributed to the strong H_2 adsorbability of Pd nanoparticles formed via Pd doping [19]. The PNB-Pd membrane showed the highest gas permeances for the smaller molecule gases (i.e. He and H_2), but its permeances for CO_2, N_2, CH_4 and SF_6 are lower than those of the PNB-PdNb membrane. This result can be ascribed to its moderate pore size which was calculated based on the NKP method (Fig S1 and S2) [39]. Among the three PNB membranes, the PNB-Nb membrane exhibited the lowest gas permeances for all tested gases. The H_2/CO_2 separation performance of the three PNB membranes were compared in Fig. 9 (b). We found that the PNB-Pd membrane showed the highest H_2 permeance (9.68×10^{-7} $mol\cdot m^{-2}\cdot s^{-1}\cdot Pa^{-1}$) and the largest

H_2/CO_2 permselectivity (17.2). This result indicates that the PNB-Pd membrane may possess the best Pd-Nb bimetallic doped network with the optimal porous structure for H_2/CO_2 separation. Fig S3 showed the H_2 and CO_2 adsorption isotherms of the three PNB networks. PNB-Pd network exhibited the highest H_2 adsorption capacities, corroborating the highest H_2 permeance and largest H_2/CO_2 permselectivity of the PNB-Pd membrane. In addition, the PNB-Nb membrane showed a high H_2/CO_2 permselectivity of 15.4, but its H_2 permeance was the lowest (4.03×10^{-7} mol·m^{-2}·s^{-1}·Pa^{-1}). On the contrary, the PNB-PdNb membrane showed a high H_2 permeance of 6.06×10^{-7} mol·m^{-2}·s^{-1}·Pa^{-1}, but its H_2/CO_2 permselectivity was the lowest (8.84). The H_2/CO_2 separation performances of the three PNB membranes are consistent with the aforementioned microporous analysis.

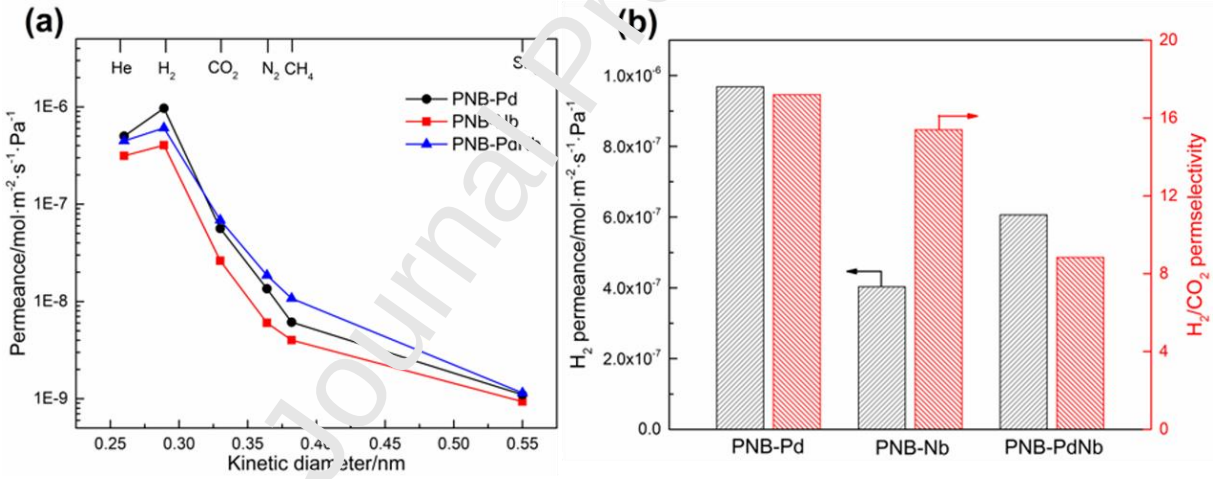

Fig. 9. (a) Gas permeance and (b) H_2/CO_2 separation performance of PNB membranes measured at 200 ºC.

To further study the transport mechanisms of gases permeation through the PNB membranes, the relationship between gas permeance and temperature was investigated. Fig. 10 is the Arrhenius plot of gas permeances, which are calculated by the following Eq. (3) and Eq. (4) [40]:

$$P = P_0 \exp\left(\frac{-\Delta E}{RT}\right) \quad (3)$$

$$lnP = -\frac{\Delta E}{RT} + lnP_0 \quad (4)$$

where P is the gas permeance, P_0 is the temperature independent parameter, R is the gas constant, T is the measured temperature and the ΔE is the activation energy.

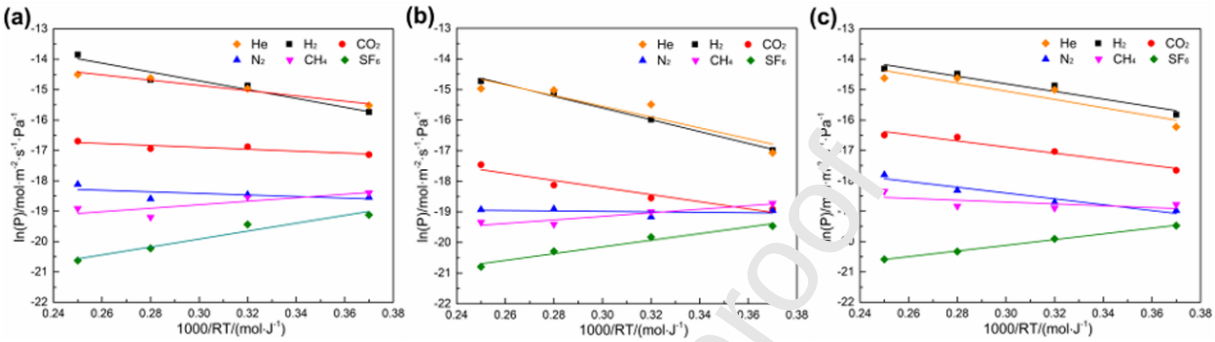

Fig. 10. Temperature dependency of gas permeances for (a) PNB-Pd, (b) PNB-Nb and (c) PNB-PdNb membranes.

Fig. 10 shows the linear fittings of *lnP* as a function of *1000/RT* with slopes equal to -ΔE (kJ·mol^{-1}) according to Eq. (4). The positive value of ΔE indicates the gas transports through a membrane is controlled by the activated diffusion mechanism, while the negative ΔE suggests the gas transportation process obeys surface diffusion mechanism [41]. The activation energies for all the tested gases permeated through the three PNB membranes were given in Table S2. The ΔE values of He, H_2, CO_2 and N_2 are positive for PNB membranes indicating those gases pass through the as-prepared membranes based on activated diffusion. A higher activation energy means higher resistance need to overcome by gas molecules through membrane pores. PNB-Nb membrane showed the higher activation energy of He and H_2 than that of PNB-Pd and PNB-PdNb membranes. This result suggests that PNB-Nb membrane forms a denser structure via the synthesis route of Nb doping priority, which is consistent with its low gas permeance. PNB membranes show the negative activation energies for CH_4 (except PNB-PdNb membrane) and SF_6. This result suggests that transportation of CH_4 and

SF_6 molecules through the membranes is controlled by the surface diffusion mechanism.

Fig. 11 compares the H_2/CO_2 separation performance (H_2 permeance and H_2/CO_2 permselectivity) of the as-prepared PNB membranes with that of the reported pure BTESE or monometallic doped BTESE membranes measured at 200 ºC. Pure BTESE-derived membranes generally exhibited a high H_2 permeance but their H_2/CO_2 permselectivities are very close to the Knudsen diffusion factor. As discussed above, monometallic doped BTESE membranes can often unilaterally improve either H_2 permeance or H_2/CO_2 permselectivity. All the PNB membranes prepared in this work showed both high H_2 permeances and good H_2/CO_2 permselectivities. Particularly, PNB-Pd membrane exhibited the excellent H_2 permeance up to $10^{-6}\times mol\cdot m^{-2}\cdot s^{-1}\cdot Pa^{-1}$ and the good H_2/CO_2 permselectivity of 17.2. In addition, the PNB-Pd membrane showed a good stability at 200 ºC for 120 h (Fig. S4). This finding may suggest that PNB membranes are possible to overcome the long-standing trade-off limitation by taking advantages of the two metals, and the PNB-Pd membrane has a great competitiveness in BTESE-derived membranes for H_2/CO_2 separation.

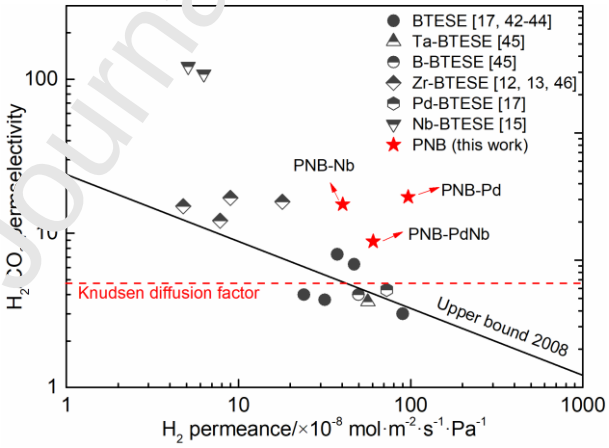

Fig.11. Comparison of H_2/CO_2 separation performance for the PNB membranes prepared in this work with that for other BTESE-derived membranes reported in literatures (BTESE [17, 42-44], Ta-BTESE [45], B-BTESE [45], Zr-BTESE [12, 13, 46], Pd-BTESE [17], Nb-BTESE [15]).

4. Conclusions

Bimetallic doped BTESE-derived organosilica membranes with three Pd-Nb doping routes were fabricated by using the sol-gel method. By tuning the different metal doping routes, the influences on the microstructure and the H_2/CO_2 separation performance of the as-prepared PNB membranes were compared. As evidenced by chemical characterization, we confirmed that Pd could exist in BTESE-derived network as nanoparticles while Nb was incorporated into the network forming Nb-O-Si covalent bonds. According to the morphological and microstructural analysis, we found that the doping route has significant influences on the resultant PNB networks (e.g. Pd particle size distribution and pore structure). The three metal doping routes results in three different PNB networks. Among the three membranes, the PNB-Nb membrane with the highest condensation degree and small-size Pd nanoparticles could show a relatively low H_2 permeance, and the PNB-PdNb membrane showed a low H_2/CO_2 permselectivity due to the larger pore size caused by the low cross-linking degree and inhomogeneous distribution of Pd nanoparticles. The PNB-Pd route was found to be optimal that the corresponding network showed the highest surface area of 335 $m^2 \cdot g^{-1}$ and the larges H_2 adsorption capacities. The superior structure and H_2 adsorption properties conferred the PNB-Pd membrane with the highest H_2 permeace ($\sim 10^{-6}$ $mol \cdot m^{-2} \cdot s^{-1} \cdot Pa^{-1}$) and highest H_2/CO_2 permselectivity (17.2), which is much higher than upper bound 2008. This work may provide novel insights for constructing high-performance metal doped organosilica membranes for H_2/CO_2 separation.

Acknowledgments

This work is supported by the National Nature Science Foundation of China (21490581), China Petroleum & Chemical Corporation (317008-6) and Guangxi Innovation Driven Development Foundation (AA17204092).

References

[1] X. Ren, T. Tsuru, Organosilica-Based Membranes in Gas and Liquid-Phase Separation, Membranes, 9 (2019) 1-24.

[2] A.P. Dral, K. Tempelman, E.J. Kappert, L. Winnubst, N.E. Benes, J.E.T. Elshof, Long-term flexibility-based structural evolution and condensation in microporous organosilica membranes for gas separation, J. Mater. Chem A. 5 (2016) 1269-1281.

[3] H.L. Castricum, G.G. Paradis, M.C. Mittelmeijer-Hazeleger, R. Kreiter, J.F. Vente, J.E. ten Elshof, Tailoring the Separation Behavior of Hybrid Organosilica Membranes by Adjusting the Structure of the Organic Bridging Group, Adv. Funct. Mater., 21 (2011) 2319-2329.

[4] A.P. Dral, J.E. ten Elshof, Organic groups influencing microporosity in organosilicas, Microporous Mesoporous Mater., (2018) 267-273.

[5] M. Kanezashi, Y. Yoneda, H. Nagasawa, T. Tsuru, K. Yamamoto, J. Ohshita, Gas permeation properties for organosilica membranes with different Si/C ratios and evaluation of microporous structures, AIChE J., 63 (2017) 1-8.

[6] E.J. Kappert, D. Pavlenko, J. Malzbender, A. Nijmeijer, N.E. Benes, P.A. Tsai, Formation and prevention of fractures in sol-gel-derived thin films, Soft Matter, 11 (2015) 882-888.

[7] M. Kanezashi, K. Yada, T. Yoshioka, T. Tsuru, Design of Silica Networks for Development of Highly Permeable Hydrogen Separation Membranes with Hydrothermal Stability, J. Am. Chem. Soc., 131 (2009) 414-415.

[8] K.-S. Chang, T. Yoshioka, M. Kanezashi, T. Tsuru, K.-L. Tung, A molecular dynamics simulation of a homogeneous organic-inorganic hybrid silica membrane, Chem. Commun., 46 (2010) 9140-9142.

[9] C. Yacou, S. Smart, J.C. Diniz da Costa, Long term performance cobalt oxide silica membrane module for high temperature H_2 separation, Energy & Environmental Science, 5 (2012) 5820-5832.

[10] P. Karakiliç, C. Huiskes, M.W.J. Luiten-Olieman, A. Nijmeijer, L. Winnubst, Sol-gel processed magnesium-doped silica membranes with improved H_2/CO_2 separation, J. Membr. Sci., 543 (2017) 195-201.

[11] M. Kanezashi, S. Miyauchi, H. Nagasawa, T. Yoshioka, T. Tsuru, Gas permeation properties through Al-doped organosilica membranes with controlled network size, J. Membr. Sci., 466 (2014) 246-252.

[12] M.T. Hove, A. Nijmeijer, L. Winnubst, Facile synthesis of zirconia doped hybrid organic inorganic silica membranes, Sep. Purif. Technol., 147 (2015) 372-378.

[13] H. Song, S. Zhao, J. Chen, H. Qi, Hydrothermally stable Zr-doped organosilica membranes for H_2/CO_2 separation, Microporous Mesoporous Mater., 224 (2016) 277-284.

[14] V. Boffa, J.E. ten Elshof, A.V. Petukhov, D.H. Blank, Microporous niobia-silica membrane with very low CO_2 permeability, ChemSusChem, 1 (2010) 437-443.

[15] H. Qi, H. Chen, L. Li, G. Zhu, N. Xu, Effect of Nb content on hydrothermal stability of a novel ethylene-bridged silsesquioxane molecular sieving membrane for H_2/CO_2 separation, J. Membr. Sci., 421-422 (2012) 190-200.

[16] M. Kanezashi, M. Sano, T. Yoshioka, T. Tsuru, Extremely thin Pd-silica mixed-matrix membranes with nano-dispersion for improved hydrogen permeability, Chem. Commun., 46 (2010) 6171-6173.

[17] H. Song, S. Zhao, J. Lei, C. Wang, H. Qi, Pd-doped organosilica membrane with enhanced gas permeability and hydrothermal stability for gas separation, J. Mater. Sci., 51 (2016) 6275-6286.

[18] M. Kanezashi, D. Fuchigami, T. Yoshioka, T. Tsuru, Control of Pd dispersion in sol-gel-derived amorphous silica membranes for hydrogen separation at high temperatures, J. Membr. Sci., 439 (2013) 78-86.

[19] S. Yun, S.T. Oyama, Correlations in palladium membranes for hydrogen separation: A review, J. Membr. Sci., 375 (2011) 28-45.

[20] M. Kanezashi, Sol-Gel-Derived Silica Membranes, John Wiley & Sons, New York, USA, 2013.

[21] A. Darmawan, J. Motuzas, S. Smart, A. Julbe, J.C. Diniz da Costa, Binary iron cobalt oxide silica membrane for gas separation, J. Membr. Sci., 474 (2015) 32-38.

[22] A. Darmawan, J. Motuzas, S. Smart, A. Julbe, J.C. Diniz da Costa, Gas permeation redox effect of binary iron oxide/cobalt oxide silica membranes, Sep. Purif. Technol., 171 (2016) 248-255.

[23] B. Ballinger, J. Motuzas, S. Smart, J.C. Diniz da Costa, Gas permeation redox effect on binary lanthanum cobalt silica membranes with enhanced silicate formation, J. Membr. Sci., 489 (2015) 220-226.

[24] B. Ballinger, J. Motuzas, S. Smart, J.C. Diniz da Costa, Palladium cobalt binary doping of molecular sieving silica membranes, J. Membr. Sci., 451 (2014) 185-191.

[25] P.H.T. Ngamou, M.E. Ivanova, C. Herwartz, N. Lühmann, A. Besmehn, W.A. Meulenberg, J. Mayer, O. Guillon, Tailoring the structure and gas permeation properties of silica membranes via binary metal oxides doping, Rsc Advances, 5 (2015) 82717-82725.

[26] H.-Y. Zhang, J.-L. Wen, Q. Shao, A. Yuan, H.-T. Ren, F.-Y. Luo, X.-L. Zhang, Fabrication of La/Y-codoped microporous organosilica membranes for high-performance

pervaporation desalination, J. Membr. Sci., 584 (2019) 353-363.

[27] H. Zhang, Y. Wei, H. Qi, Palladium-niobium bimetallic doped organosilica membranes for H_2/CO_2 separation, Microporous Mesoporous Mater., (2020) 110279.

[28] H. Qi, J. Han, N. Xu, Effect of calcination temperature on carbon dioxide separation properties of a novel microporous hybrid silica membrane, J. Membr. Sci., 382 (2011) 231-237.

[29] D.-T. Phan, G.-S. Chung, Characteristics of resistivity-type hydrogen sensing based on palladium-graphene nanocomposites, Int. J. Hydrogen Energy, 39 (2014) 620-629.

[30] Y. Wei, H. Zhang, J. Lei, H. Song, H. Qi, Controlling pore structures of Pd-doped organosilica membranes by calcination atmosphere for gas separation, Chin. J. Chem. Eng., (2019) 3036-3042.

[31] R. Al-Oweini, H. El-Rassy, Synthesis and characterization by FTIR spectroscopy of silica aerogels prepared using several $Si(OR)_4$ and $R''Si(OR')_3$ precursors, J. Mol. Struct., 919 (2009) 140-145.

[32] P.T. Ngamou, J.P. Overbeek, R. Kreiter, H.M.V. Veen, J.F. Vente, I.M. Wienk, P.F. Cuperus, M. Creatore, Plasma-deposited hybrid silica membranes with a controlled retention of organic bridges, J. Mater. Chem A, 1 (2013) 5567-5576.

[33] G. Gong, H. Nagasawa, M. Kanezashi, T. Tsuru, Tailoring the Separation Behavior of Polymer-Supported Organosilica Layered Hybrid Membranes via Facile Post-Treatment Using HCl and HN_3 Vapors, ACS Appl. Mater. Interfaces, 8 (2016) 11060-11069.

[34] H. Song, Y. Wei, H. Qi, Tailoring pore structures to improve the permselectivity of organosilica membranes by tuning calcination parameters, J. Mater. Chem A, 5 (2017) 24657-24666.

[35] H. Yue, X. Yan, S.J. Ding, H.L. Lu, Q.Q. Sun, D.W. Zhang, Z. Chen, Thermal stability of atomic-layer-deposited ultra-thin niobium oxide film on Si (1 0 0), Appl. Surf. Sci., 257 (2011) 7305-7309.

[36] S. Damyanova, L. Dimitrov, L. Petrov, P. Grange, Effect of niobium on the surface properties of Nb_2O_5-SiO_2-supported Mo catalysts, Appl. Surf. Sci., 214 (2003) 68-74.

[37] M.S.P. Francisco, R. Landers, Y. Gushikem, Local order structure and surface acidity properties of a Nb_2O_5/SiO_2 mixed oxide prepared by the sol-gel processing method, J. Solid State Chem., 177 (2004) 2432-2439.

[38] M. Thommes, K. Kaneko, A.V. Neimark, J.P. Olivier, F. Rodriguez-Reinoso, J. Rouquerol, K.S.W. Sing, Physisorption of gases, with special reference to the evaluation of surface area and pore size distribution (IUPAC Technical Report), Pure Appl. Chem., 87 (2015) 1051-1069.

[39] H. Nagasawa, T. Niimi, M. Kanezashi, T. Yoshioka, T. Tsuru, Modified gas-translation model for prediction of gas permeation through microporous organosilica membranes, AIChE

J., 60 (2015) 4199-4210.

[40] V. Boffa, D.H.A. Blank, J.E.T. Elshof, Hydrothermal stability of microporous silica and niobia-silica membranes, J. Membr. Sci., 319 (2008) 256-263.

[41] T. Yoshioka, E. Nakanishi, T. Tsuru, M. Asaeda, Experimental studies of gas permeation through microporous silica membranes, AIChE J., 47 (2001) 2052-2063.

[42] N. Moriyama, H. Nagasawa, M. Kanezashi, K. Ito, T. Tsuru, Bis(triethoxysilyl)ethane (BTESE)-derived silica membranes: pore formation mechanism and gas permeation properties, J. Sol-Gel Sci. Technol., 86 (2018) 63-72.

[43] H.F. Qureshi, A. Nijmeijer, L. Winnubst, Influence of sol-gel process parameters on the micro-structure and performance of hybrid silica membranes, J. Membr. Sci., 446 (2013) 19-25.

[44] H.L. Castricum, H.F. Qureshi, A. Nijmeijer, L. Winnubst, Hybrid silica membranes with enhanced hydrogen and CO_2 separation properties, J. Membr. Sci., 488 (2015) 121-128.

[45] H.F. Qureshi, R. Besselink, J.E.T. Elshof, A. Nijmeijer, L. Winnubst, Doped microporous hybrid silica membranes for gas separation, J. Sol-Gel Sci. Technol., 75 (2015) 180-188.

[46] M.T. Hove, M.W.J. Luiten-Olieman, C. Huiskes, A. Nijmeijer, L. Winnubst, Hydrothermal stability of silica, hybrid silica and Zr-doped hybrid silica membranes, Sep. Purif. Technol., (2017) 48-53.

Conflict of Interest Statement

The authors declare that they have no known competing financial interests or personal relationships that could have appeared to influence the work reported in this paper.

Graphical abstract

The metal doping routes significantly influence the microstructure of PNB networks and gas separation performance of the PNB membranes.